RASĀYAN *J. Chem.*
Vol. 19 | No. 1 | 36-47 | January-March | 2026
ISSN: 0974-1496 | e-ISSN: 0976-0083 | CODEN: RJCABP
http://www.rasayanjournal.com
http://www.rasayanjournal.co.in

SYNERGISTIC EFFECTS OF pH ON COPPER DOPING IN NICKEL OXIDE NANOPARTICLES FOR ENHANCED PHOTOCATALYTIC DEGRADATION OF ACID RED DYE

Venkata Nagendra Kishore T., K. Jaya Prasanthi✉ and Jayasree Komara
Department of Chemistry, AU College of Science and Technology, Andhra University, Visakhapatnam-530003, India
✉Corresponding author: dr.kjprasanthi@andhrauniversity.edu.in

ABSTRACT
The purpose of this study is to use copper-doped nickel oxide nanoparticles (Cu-NiO NPs) as a photocatalyst to remove the harmful acid red dye. Cu-NiO NPs were prepared hydrothermally, and their properties were investigated using XRD, SEM, EDS, BET, UV-Vis, TGA, XPS and FTIR techniques. The average particle size of NiO NPs and Cu-NiO NPs is 14.58nm and 6.63nm, respectively. The UV absorbance studies showed a strong absorption at 370nm and 390nm, respectively, and the band gap energy values of NiO NPs and Cu-NiO NPs are 2.51eV and 2.45eV. The doping of copper into the Nickel oxide nanoparticles had decreased the band gap energy, resulting in Cu-NiO NPs showing more effectiveness in photocatalytic dye degradation. This study was used to optimize the agitation period, adsorbent dose, solution pH and starting concentration of acid red dye solution during the adsorption process. The agitation length of 115 minutes, the Cu-NiO NPs dose of 0.1 g, the solution pH of 9 and the acid red dye starting concentration of 10 mg/L resulted in a 100% acid red dye degradation rate.
Keywords: Cu-NiO NPs, Acid Red Dye, Characterizations, Photocatalytic Dye Degradation, Catalyst.
RASĀYAN *J. Chem.*, Vol. 19, No.1, 2026

INTRODUCTION

Textile dye effluents are major environmental contaminants due to their toxicity, non-biodegradability, and resistance to conventional treatment methods. Even at concentrations below 1 ppm, dyes remain visually detectable and significantly impact aquatic ecosystems. While existing techniques like chemical precipitation, electrocoagulation and adsorption merely transfer pollutants between phases, they often lead to secondary pollution.[1-4] Hence, identifying an efficient wastewater treatment method to eliminate colour from textile effluents is imperative. Various chemical and physical techniques, including chemical precipitation, electrocoagulation[5,6] and adsorption on activated carbon, are commonly employed. However, these approaches merely transfer contaminants from one phase to another rather than degrading them, thereby introducing secondary pollution and necessitating additional treatments.[7-8] Advanced Oxidation Processes (AOPs), particularly photocatalysis, offer a more effective alternative by generating hydroxyl radicals that degrade organic pollutants.[9,10] Among the various remediation techniques, semiconductor photocatalysis has gained substantial attention in water treatment.[11] Nanoscience plays a pivotal role in addressing emerging environmental and biomedical challenges. Nanoparticles are being extensively utilised as photocatalysts, antibacterial agents, anti-inflammatory compounds, antifungal agents and antimicrobial filters.[12] Efficient and straightforward photocatalytic systems are now preferred for degrading organic dyes while minimizing toxic chemical waste. Notably, metal oxide nanoparticles (NiO, CuO, MgO, TiO_2 , ZnO, etc.) exhibit remarkable chemical and physical properties, including nanoscale dimensions, high surface area-to-volume ratio, controlled morphology and superior light absorption, making them widely applicable across various industries.[13] Currently, photocatalytic degradation of organic dyes in wastewater has emerged as an effective strategy for pollution control. Semiconductor oxides such as TiO_2 , ZnO, NiO and MgO facilitate the oxidation-reduction reactions necessary to break down organic pollutants into less harmful substances.[14] A photocatalyst is defined as a substance capable of decomposing and eliminating contaminants from surfaces or the environment. Among the available, Cu-doped NiO nanoparticles (Cu-NiO NPs) have demonstrated exceptional

chemical stability and efficiency in breaking molecular bonds, making them a promising material for environmental remediation.[15] These nanoparticles have shown great potential in removing non-biodegradable organic pollutants and heavy metals from wastewater as well as in disinfecting drinking water by neutralizing bacteria and viruses.[16-18] Beyond environmental applications, Cu-doped NiO-NPs have been employed in diverse technological fields, including cathode batteries[19], fuel cells[20] and catalysis.[21] However, the high resistivity of NiO remains a limitation in some applications. To overcome this, doping with monovalent impurities such as copper (Cu) has been employed to enhance NiO NPs' electrical and thermal conductivity while improving their corrosion resistance.[22,23] Moreover, Cu-doped NiO-NPs have demonstrated significant biomedical applications, including anticancer, antiparasitic, antifungal and antibacterial activities along with their utility in food packaging and wound dressing.[24] In the present work, copper-doped nickel oxide nanoparticles (Cu–NiO NPs) were prepared via a hydrothermal route, which represents a sustainable and mild synthesis technique. This process avoids the use of elevated temperatures and toxic reducing agents while enabling controlled formation of nanoparticles. Owing to its operational simplicity, reproducibility, and eco-friendly nature, the hydrothermal approach provides an efficient and economical alternative to traditional physical and chemical synthesis methods.

EXPERIMENTAL

Materials Used

Nickel chloride hexahydrate ($NiCl_2 \cdot 6H_2O$) from Sigma-Aldrich, Sodium hydroxide (NaOH) from Merck, Cupric chloride ($CuCl_2$), Ethanol and Ascorbic acid. Doubled-distilled water was used throughout the studies, and analytical-grade chemicals were used.

Synthesis of Cu-doped NiO

1.78 g of $NiCl_2$ was dissolved in 30 mL of deionized water and kept for 10 min. Then, 30 mL of 0.12gm of NaOH solution was gradually added to the above solution. Then the mixture was kept on the hotplate, allowed to stir and heated at 60°C for 30 min. To the above mixture, 0.4 g of $CuCl_2$ and 30 mL was added and kept for 30 min stirring, to this a pinch of ascorbic acid was added and kept for one hour stirring. Then it is transferred into a Teflon stainless steel beaker and placed in a muffle furnace at 180 °C for 4 hours. After this, it was allowed to cool until it reached room temperature and filtered, washed the obtained mixture with water and ethanol and finally dried it in a hot air oven at 60°C for 8 hours, and the product was ground to a fine powder for further analysis. In the absence of $CuCl_2$, the same procedure was repeated in synthesising the Nickel oxide nanoparticles (NiO NPs).

Characterization

In this present study the characterization were carried out using the following techniques X-ray diffraction (XRD) study was carried out with instrument D8 Bruker Advance A25, Cu tube using its wavelength with Cu-Kα =1.5418 A° in the range 2θ from 10° - 80° to determine the interplanar spacing of the nanoparticles, Fourier transformation Infrared spectroscopy (FTIR) analysis with the instrument ATR-FTIR spectrophotometer with make Bruker, model Alpha-II, Air-cooled, 12V, 20W Beam Splitter: Zinc Selenide (ZnSe) in the range 4000-500cm^{-1}, Quantachrome NOVA touch 4 LX instrument was used for BET analysis using nitrogen isotherms at 77 K, Tecnai T20, 200Kev, FEI electron microscope was used for the TEM analysis, The XPS (X ray photoelectron spectroscopy) analysis was carried out with the instrument Omicron ESCA make Oxford Germany. TGA was carried out using the Hitachi STA 7300 model from 30 °C to 1000 °C. The lateral size and morphology of the nanomaterials were described by using a scanning electron microscope (FE-SEM, Quanta 450 FEG, FEI, USA; and SEM, Hitachi SU1510, Japan) at an operating voltage of 10–30 kV.

Measurement of Photocatalytic Activity

Photocatalytic degradation studies were performed under normal atmospheric conditions at pH levels of 5, 7, and 9. A Philips mercury UV-A lamp (365 nm) equipped with four 15 W tubes served as the irradiation source. For each experiment, 30, 50 and 100 mg of the Cu–NiO catalyst were dispersed in 100 mL of aqueous acid red dye solution (10 mg L^{-1}).

Before illumination, the suspension was magnetically stirred in the dark for 30 minutes to achieve adsorption–desorption equilibrium between the dye molecules and the catalyst surface. During the photoreaction, aliquots (≈3 mL) were periodically withdrawn and centrifuged to remove catalyst particles. The residual dye concentration in the supernatant was analyzed by recording the absorbance at 510 nm using a UV–Vis spectrophotometer.

$$\text{Efficiency}(\%) = \left(\frac{C^0_{AR} - C_{AR}}{C^0_{AR}}\right) X\ 100 \qquad (1)$$

Where C^0_{AR} represents the initial concentration of the acid red dye and C_{AR} Denotes the concentration at a given irradiation time. The change in dye concentration with respect to exposure time under UV illumination was evaluated by UV–Vis spectrophotometry, using a pre-established calibration curve to quantify the remaining dye in the solution.

Characterization Techniques

X-Ray Diffraction Analysis

The XRD analysis is used to identify the crystalline structure of the synthesized material. The existence of strong and sharp diffraction peaks of the Nickel Oxide (NiO NPs) with 2θ values[25] found to be 19.17 °, 31.75°, 33.22°, 38.64 °, 45.52 °, 59.50 °, 62.42 °,75.2 ° and Copper doped Nickel oxide (Cu-NiO NPs) were observed with 2θ values 19.27 °, 33.44 °, 38.48 °, 59.57 °, ,62.3 °, and 75.6 ° as shown in Fig.-1. The observed diffraction peaks correspond to the characteristic reflections of the cubic phase of nickel oxide (NiO), which is consistent with previously reported data and the standard JCPDS card No. 45-0937.[26] The slight variation in the 2θ values is observed due to the doping of copper metal into the NiO nanoparticles. There are no other peaks observed in between pure NiO NPs and Cu-NiO NPs, confirming that it is free from

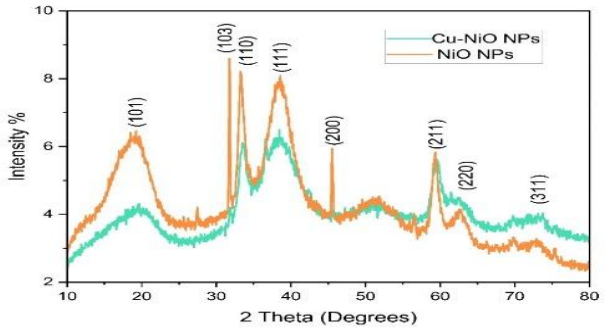

Fig.-1: XRD Patterns of Prepared NiO and Cu-NiO NPs

Impurities. The average crystalline size(D) of hydrothermally prepared material was measured by the Debye-Scherrer formula Eqn (2), and the average crystalline size of the NiO nanoparticles is obtained as 14.58nm, and the Cu- doped NiO is calculated and found to be 6.6nm. There are no other peaks observed between peaks, confirming that these are free from impurities.

$$D = \frac{k\lambda}{\beta \text{Cos}\theta} \qquad (2)$$

In this equation, λ denotes the wavelength of the X-ray radiation, k is the Scherrer constant (taken as 0.94), β represents the full width at half maximum (FWHM) of the diffraction peak, and θ corresponds to the Bragg diffraction angle.

Fourier Transform Infrared (FTIR) Spectral Analysis

Figure-2 presents the FTIR spectra of pure and Cu-doped NiO nanoparticles. The undoped NiO sample exhibited several prominent absorption bands at 3637, 3376, 1650, 1336, 1040, 625, and 506 cm^{-1}. Upon copper incorporation, a slight shift toward lower vibrational frequencies was observed, suggesting that doping did not alter the basic NiO lattice structure. The broad absorption band between 650 and 500 cm^{-1} corresponds to the Ni–O stretching vibrations, and its breadth indicates the nanocrystalline nature of the

oxide powders.[27] The broad feature near 3376 cm^{-1} is attributed to O–H stretching vibrations, while the weak band at approximately 1650 cm^{-1} arises from H–O–H bending modes, both resulting from adsorbed water molecules during FTIR pellet preparation in ambient air. These peaks confirm slight surface hydration and the presence of hydroxyl groups from precursor residues. Additionally, the absorption observed around 1040 cm^{-1} can be assigned to C–O stretching vibrations, indicating trace organic species or residual carbonates.

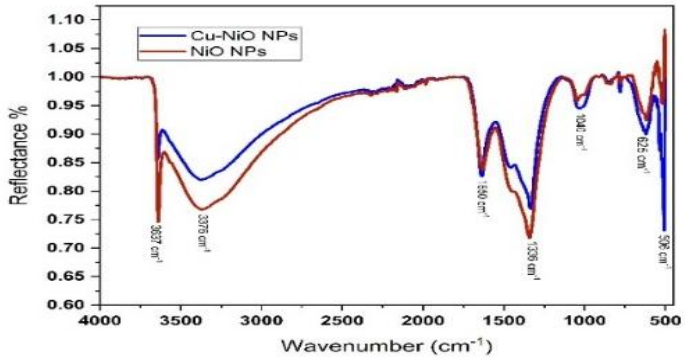

Fig.-2: FTIR Patterns of Prepared NiO and Cu-NiO NPs

Scanning Electron Microscopy

The surface morphology of the synthesized pure NiO and Cu-doped NiO nanoparticles was investigated using scanning electron microscopy (SEM) at magnifications of 1500×, 1000×, 500× and 50×. The SEM images in Fig.-3 revealed that the nanoparticles were well-dispersed, exhibiting a cubical shape with high crystallinity.[28] Both the pure NiO NPs and Cu-NiO NPs samples displayed comparable morphological characteristics. However, some degree of agglomeration was observed. This is likely due to the aggregation of smaller particles forming nanoparticle clusters. This observation is in close agreement with previous studies, which reported an average particle size distribution of approximately 18nm. Notably, the pure NiO nanoparticles appeared smaller in size**,** whereas Cu doping resulted in a relatively larger particle size. This finding correlates well with X-ray diffraction (XRD) analysis**,** which confirmed an increase in particle size upon Cu incorporation into NiO.

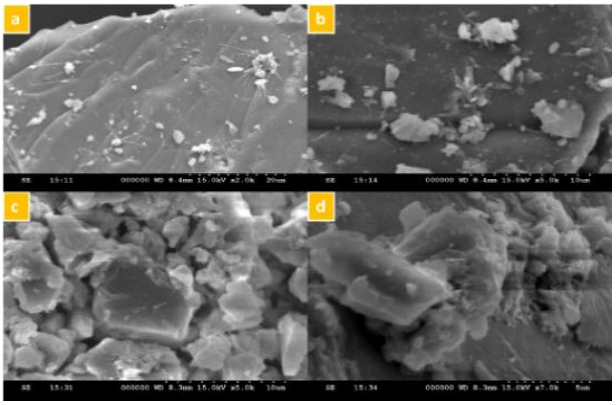

Fig.-3: SEM Images (a, b) NiO NPs (c, d) Cu-NiO NPs

Energy Dispersive X-Ray Spectroscopy Analysis (EDS)

The elemental composition of the synthesized Cu–NiO nanoparticles was analyzed using Energy Dispersive X-ray Spectroscopy (EDS) integrated with a Quanta 450 FEG system (USA). Additionally, spectral signals corresponding to Nickel, Oxygen, and Copper were detected. The elemental composition of pure Nickel and Oxygen was obtained as 47.90 and 26.60 by weight percentage in NiO NPs, and after doping with copper, the obtained Cu-NiO NPs contain Copper, Nickel and Oxygen as 2.75, 29.14 and 34.45 by weight percentage, respectively.[29]

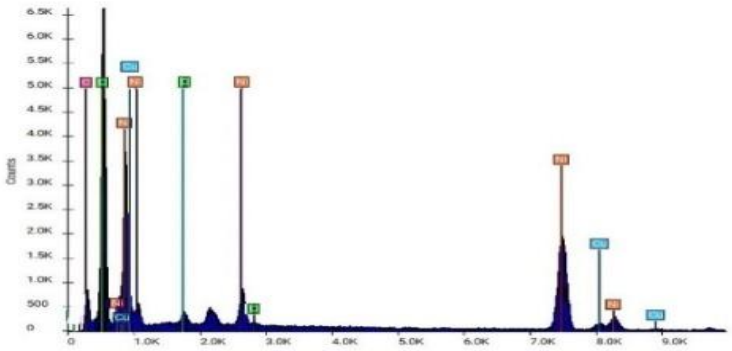

Fig.-4: EDS Analysis of Cu-NiO NPs

Transmission Electron Microscope

The morphological characteristics and particle dimensions of the Cu–NiO nanoparticles were examined using Transmission Electron Microscopy (TEM). Representative TEM micrographs. The sample is presented in Fig.-5(a–e). The TEM image of the NiO NPs is obtained with a diameter of 38.1nm after doping the Cu-NiO NPs, showing uniform particles with a diameter of about 29.3 nm. The SAED pattern given in Fig.-5f shows that the obtained Cu-NiO NPs are crystalline in nature. Noticed that the mean particle size determined by TEM values of Cu-NiO NPs was concurred with XRD crystalline size.

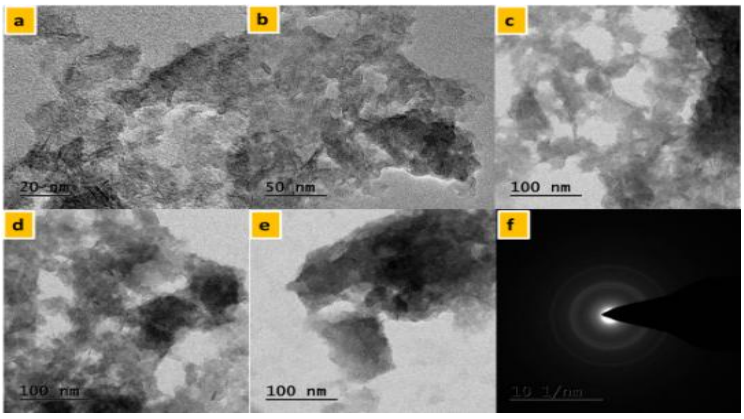

Fig.-5: (a-e) TEM Images and (f) SAED Pattern of Cu-NiO NPs

Brunauer–Emmett–Teller Adsorption (BET)

The textural properties of NiO and Cu–NiO nanoparticles were evaluated from nitrogen adsorption–desorption isotherms obtained through Brunauer–Emmett–Teller (BET) surface analysis. The specific surface areas of NiO and Cu–NiO were determined to be 109.36 and 114.86 m^2/g^{-1}, respectively. Correspondingly, the total pore volumes were calculated as 0.0241 and 0.0273 cm^3g^{-1}. The N_2 adsorption-desorption of NiO and Cu-NiO NPs shows a unique type-IV isotherm. For the NiO and Cu-NiO NPs, the average pore diameter was measured to be 3.05887 nm and 3.4179 nm, respectively. From the graph(Fig.-6), it is evident that the volume adsorbed @STP (cc/g) is increased in Cu-NiO NPs, indicating that the surface area is increased by nearly 5 per cent after doping which resulting in more catalytic activity.

X-Ray Photoelectron Spectroscopy analysis

The XPS analysis for the NiO and Cu-NiO NPs were made and the binding energies values for NiO NPs were observed for O 1s is 530 eV and Ni $2p_{3/2}$ are 855 eV and for Cu-NiO NPs the binding energy for the Cu $2p_{3/2}$, Cu $2p_{1/2}$ is obtained at 931.5 eV and 975 eV, Ni $2p_{3/2}$ and Ni $2p_{1/2}$ were observed 855 and 873.5 eV and O 1s is 529.5, shown in Fig.-7 (a-d)the peaks obtained in XPS binding energy is good agreement with the elements composition EDS analysis indicating that no other additional elements were involved.[30]

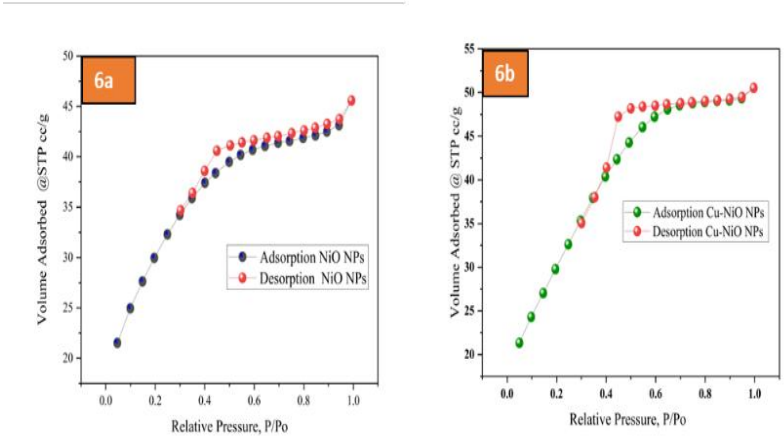

Fig.-6: a and b represent the Adsorption/ Desorption of NiO and Cu-NiO Nanoparticles

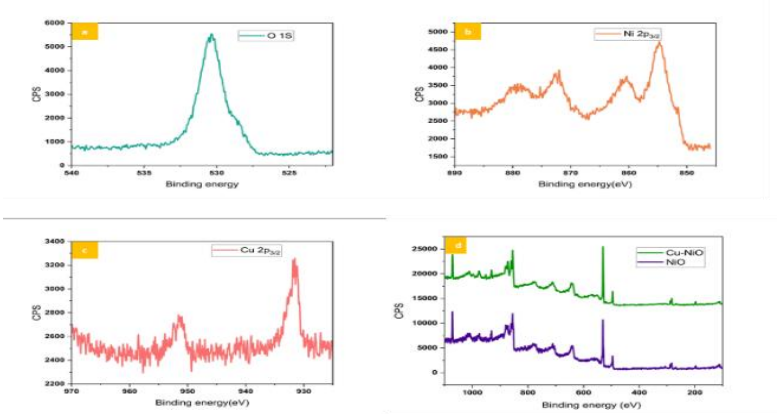

Fig.-7: XPS Data a) O 1s b) Ni 2p3/2 c) Cu 2p3/2 d) Cu-NiO NPs and NiO NPs

Thermogravimetric Analysis

The thermal stability of the synthesized Cu–NiO nanoparticles was evaluated through thermogravimetric (TG) analysis, and the resulting TG curve is presented in Fig.-8. The TG curve exhibits discrete weight losses at different temperature ranges. The first decomposition occurs between 35°C and 109°C, with an endothermic peak at 74°C, corresponding to the Loss of lattice water. A significant weight loss is observed from room temperature to 321°C, with a total mass reduction of 17.7%, attributed to the removal of water molecules present in the internal molecular lattice. The strong weight loss was noticed in the decomposition process through multiple stages of hydrothermally prepared Cu-NiO NPs at 1.77% (2.154mg), 15.36% (1.823mg) and 6.8% (1.699gm mg). The thermal decomposition is completed at 792°C, after which the Cu-NiO NPs remain as the final product with no further weight loss. For comparison of Cu-NiO NPs, the TG curves of annealed NiO at 321°C were also analyzed.[31] The results show that Cu-NiO NPs exhibit greater thermal stability compared to undoped NiO NPs.

UV-Visible Spectral Analysis

UV-Vis spectral analysis has been done for the prepared samples of bare NiO and Cu-NiO NPs, and this was shown in Fig.-9. NiO NPs show an adsorption edge at 370 nm, while Cu-NiO NPs show an absorption edge above 390 nm due to the doping of copper. The Band gap energy for the synthesized NiO NPs was found to be 2.51eV. Cu-NiO NPs, which showed an absorption edge at 390 nm and the band gap energy was found to be 2.45 eV. The decrease in the band gap energy indicates that it can show more catalytic activity. The structural and physicochemical properties of the synthesized NiO-NPs and Cu-NiO NPs were analyzed using various techniques like XRD, SEM, TEM, EDS, FTIR, UV-Vis and BET analysis results are shown in Table-1.

Table-1: Characterizations Data of the Synthesized NiO and Cu-NiO NPs

Sample	Crystal size (nm)	Particle size(nm)	Band gap energy (eV)	Surface area (m^2/gm)	Thermal weight Loss (%)
NiO	14.58	38.1	2.51	109.36	22
Cu-NiO	6.63	29.3	2.45	114.86	15.36

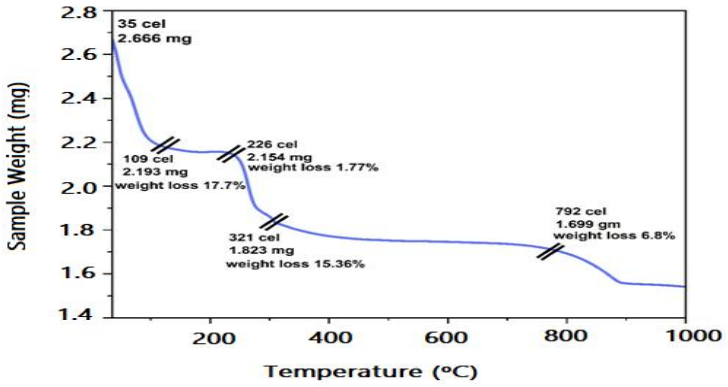

Fig.-8: Plots of TGA of Cu-NiO NPs Ranging from 0°C -1000°C

RESULTS AND DISCUSSION

Photocatalytic Degradation of Acid Red dye

The photocatalytic activity of the synthesized NiO and Cu-NiO NPs was analyzed under visible light irradiation against Acid Red (AR) dye at pH 9. Initially, the photocatalytic experiment was carried out with bare NiO NPs and found to be a 38.6% degradation rate in 150 min. As we expected in the enhancement of degradation rate, further testing was conducted with Cu-NiO NPs at similar conditions of 50 mg catalyst loading, 10 ppm and showed better photocatalytic performance than NiO. To achieve complete degradation of the Acid Red (AR) dye using the synthesized Cu–NiO NPs, optimization of key experimental parameters such as pH, catalyst dosage and initial dye concentration was essential.

Effect of pH on AR Degradation

The degradation efficiency of AR dye increases with pH, showing 25.74% degradation at pH 5, 34.17% at pH 7, and 52.87% at pH 9 shown in Fig.-10 (a, b, c). This trend suggests that alkaline conditions favour dye degradation, likely due to enhanced hydroxyl radical (•OH) formation and improved oxidation potential. In acidic conditions, fewer hydroxyl radicals may be available, limiting degradation efficiency. To further optimize the process, increasing the pH value slightly beyond 9 could enhance degradation, although excessively high pH levels (>11) might stabilize the dye or interfere with catalyst activity. Additionally, optimizing reaction time and catalyst dosage is crucial as excessive amounts may lead to radical scavenging and reduced efficiency. Since pH 9 has shown the highest degradation in this case, fine-tuning the reaction conditions and incorporating advanced oxidation methods could lead to even better results.

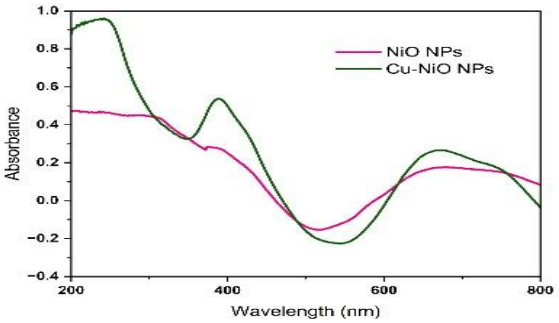

Fig.-9: Plots of UV-Visible Spectrum of NiO NPs and Cu- NiO NPs

Effect of Initial Dye Concentration

The effect of the initial concentration of Acid Red (AR) dye on the photocatalytic efficiency of Cu–NiO nanoparticles was examined under optimized pH conditions with an irradiation duration of 160 minutes. The dye concentration was varied between 5 and 20 ppm to evaluate its influence on the degradation rate. Before illumination, each dye–catalyst suspension was stirred in the dark for 30 minutes to reach adsorption–desorption equilibrium, during which approximately 25% of the dye was removed regardless of the initial concentration. Upon visible-light irradiation, complete degradation of the 5ppm solution was achieved within 90 minutes, while the 20ppm solution required about 150 minutes for full decomposition. As illustrated in Fig.-10(d), the photocatalytic efficiency decreased progressively with increasing.

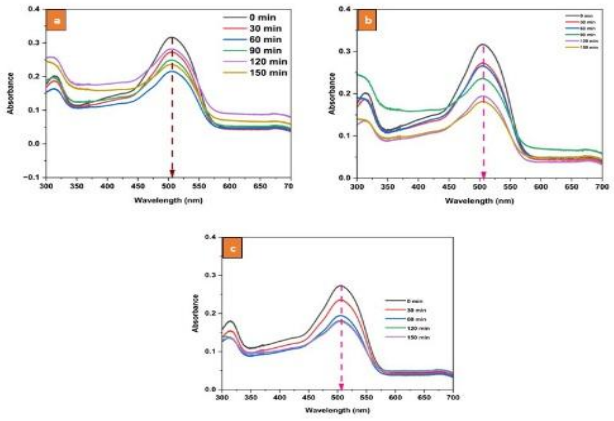

Fig.-10 (a,b,c) shows the Degradation of Acid Red Dye at Ph-5, 7 and 9, respectively

Dye concentration. This inverse relationship can be attributed to the higher number of dye molecules occupying active sites on the catalyst surface, which restricts light penetration and suppresses the formation of reactive hydroxyl radicals. Consequently, at elevated dye concentrations, reduced availability of hydroxyl radicals leads to a decline in overall photocatalytic activity.

Effect of Catalyst Dose

The influence of catalyst dosage on the photocatalytic degradation of Acid Red dye was examined while maintaining all other experimental parameters constant. The study was conducted using different Cu–NiO NPs loadings of 30 mg, 40 mg and 100 mg at a fixed dye concentration of 10 mg/L. The complete degradation of the dye was achieved in 150, 155 and 115 minutes, respectively, as presented in Fig.-10(e). An increase in catalyst dosage enhanced both the photon absorption capacity and the number of dye molecules degraded. This improvement in degradation efficiency can be attributed to the greater availability of active sites and better surface coverage provided by the higher catalyst loading. Furthermore, uniform dispersion of Cu–NiO NPs at elevated concentrations facilitates more effective interactions between dye molecules and reactive species, thereby accelerating the photocatalytic process.

Influence of pH on Photocatalytic Degradation

Among the various parameters governing photocatalytic reactions on particulate surfaces, pH is one of the most critical factors. The pH of the reaction medium strongly influences the surface charge properties of the photocatalyst as well as the degree of nanoparticle aggregation. Consequently, it affects both the physicochemical behaviour of dye molecules and the reaction pathways that govern their degradation. The principal mechanisms include hydroxyl radical attack, direct oxidation by photogenerated holes, and direct reduction by conduction band electrons. Under visible light irradiation, the semiconductor photocatalyst absorbs photons and generates electron–hole pairs on its surface. The photogenerated holes, possessing strong oxidative potential, can directly oxidise dye molecules or react with surface hydroxyl groups (OH^-) to yield hydroxyl radicals (·OH). Simultaneously, electrons in the conduction band may

reduce adsorbed oxygen species, leading to the formation of reactive oxygen radicals ($\cdot O_2^-$). These highly reactive oxidative species ($\cdot OH$ and $\cdot O_2^-$) subsequently interact with Acid Red dye molecules, resulting in the breakdown of the chromophoric structure and the mineralisation of the dye into harmless end products such as carbon dioxide and water.

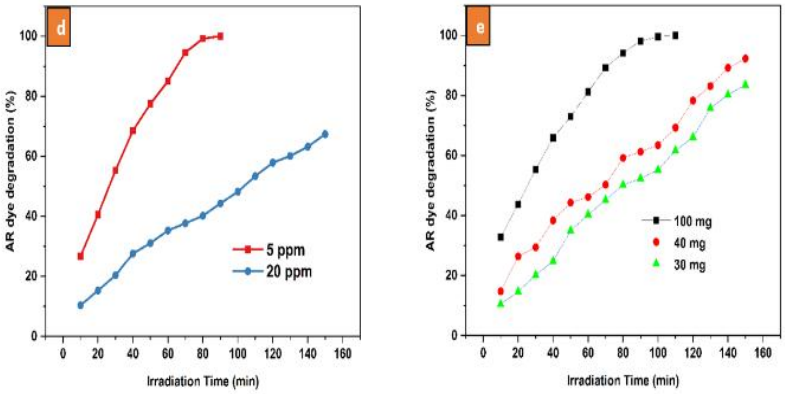

Fig.-10 (d,e): Initial Concentration of Dye Degradation after Loading the Catalyst Respectively

$$\text{Cu-NiO NPs} + h\nu \rightarrow e^-_{CB} + h^+_{VB} \qquad \text{Eqn. (3)}$$

$$h^+_{VB} + \text{Dye} \rightarrow \text{Dye}^{\cdot+} \qquad \text{Eqn.(4)}$$

$$OH^{\cdot} + \text{Dye} \rightarrow \text{degradation of the dye} \rightarrow CO_2 + H_2O \qquad \text{Eqn.(5)}$$

The degradation of Acid Red dye using different metal-doped nanoparticles, which were synthesized through deposition–precipitation, sol-gel, and hydrothermal methods, is shown in Table-1. The most effective catalyst was Cu–NiO NPs synthesized hydrothermally, achieving complete (100%) dye degradation within 2.5 hrs. These findings underscore the influence of dopant type, synthesis method and activation conditions on the photocatalytic efficiency of nanoparticles.

Table-1: Showing the Data of Differently Synthesized Metal Oxide Nanoparticles Formation and their Percentage of Dye Degradation

S. No.	Nanoparticle	Metal doped	Method used	Particle Size(nm)	Degradation (%)	Time for degradation (Hrs)	References
1	Au-TiO_2	Au	Deposition-Precipitation	10-15	48	4	[32]
2	Au-TiO_2-PMS	Au	Deposition-Precipitation	10-15	40	4	[32]
3	Au-TiO_2-PDS	Au	Deposition-Precipitation	10-15	35	4	[32]
4	Au-TiO_2-H_2O_2	Au	Deposition-Precipitation	10-15	Negligible	4	[32]
5	Ag-TiO_2-PMS	Ag	Deposition-Precipitation	10-20	55	5-7	[33]
6	Au-TiO_2-PDS	Ag	Deposition-Precipitation	10-20	58	5-7	[33]
7	Au-TiO_2- H_2O_2	Ag	Deposition-Precipitation	10-20	Negligible	5-7	[33]
8	MgFeO	Mg	Sol-gel	20	72.7	3.1	[34]
9	Zn-TiO_2 (in dark)	Zn	Sol-gel	3.2	99	3	[35]
10	Cu-NiO	Cu	Hydrothermal	18	100	2.5	Current study

CONCLUSION

The successful incorporation of Copper into Nickel oxide nanoparticles (Cu-NiO NPs) for the formation of Cu-NiO NPs through a hydrothermal approach. Further, the optical, electrical, thermal and structural properties of synthesised Cu-NiO NPs were examined. The photocatalytic degradation of AR dye in the visible light irradiation using NiO NPs and Cu-NiO NPs was examined, and these results showed that the synthesised Cu-NiO NPs were more effective for acid dye degradation. The degradation studies were observed at pH-5, 7, and 9. At pH-9, the photocatalytic dye degradation is found to be 100% within a span of 115 minutes. Therefore, the Cu-NiO NPs are suitable for the degradation of acid red dye for wastewater treatment on a large scale.

ACKNOWLEDGEMENTS

The authors are deeply thankful to the Department of Chemistry, Andhra University, Visakhapatnam, for providing state-of-the-art research facilities and continuous encouragement throughout this work. Special acknowledgement is extended to Bio Enviro Chemical Solutions Pvt. Ltd., and the Indian Institute of Petroleum and Energy, Visakhapatnam, for their valuable technical inputs, instrumentation support and collaborative assistance, which played a pivotal role in the successful realisation of this research.

CONFLICT OF INTEREST

The authors declare that there is no conflict of interest.

AUTHOR CONTRIBUTIONS

The present work is related to *SDG-6: Clean Water and Sanitation*. All the authors contributed significantly to this manuscript, participated in reviewing/editing and approved the final draft for publication. The research profile of the authors can be verified from their ORCID ids, given below:

Venkata Nagendra Kishore https://orcid.org/0009-0006-3552-878X
K. Jaya Prasanthi https://orcid.org/0009-0000-3308-3429
Jayasree Komara https://orcid.org/0009-0003-3510-9604

Cite this article as: Venkata Nagendra Kishore T. *et al*., *Rasayan J. Chem.*, 19(1), 36-47(2026), https://doi.org/10.317 88/RJC.2026.1919435

REFERENCES

1. M. M. Islam, A. R. Aidid, J. N. Mohshin, H. Mondal, S. Ganguli, and A. K. Chakraborty. *Cleaner Chemical Engineering,* **11,** 100165(2025), https://doi.org/10.1016/j.clce.2025.100165
2. M. Kumar, V. P. Singh, S. B. Bhat, and R. Kumar. *Discover Environment,* **3(1),** 132(2025), https://doi.org/10.1007/s44274-025-00337-0
3. T. A. Aragaw. *Journal of Hazardous Materials Advances,* **16,** 100493(2024), https://doi.org/10.1016/j.hazadv.2024.100493
4. A. P. Periyasamy. *Sustainability,* **16(2),** 495(2024), https://doi.org/10.3390/su16020495
5. M. R. Al-Kilani. *Journal of Water Process Engineering*, Article **2804343**(2025), https://doi.org/10.1016/S1944398624204343
6. A. M. Zafar, A. Naeem, M. A. Minhas, M. J. Hasan, S. Rafique, and A. Ikhlaq. *Total Environment Advances,* **9,** 200087(2024), https://doi.org/10.1016/j.teadva.2023.200087
7. G. S. Sree, S. M. Botsa, B. J. M. Reddy, and K. V. B. Ranjitha. *Arabian Journal of Chemistry,* **13(4)**, 5137(2020), https://doi.org/10.1016/j.arabjc.2020.02.012
8. S. A. Khan, S. Shahid, B. Shahid, U. Fatima, and S. A. Abbasi. *Biomolecules,* **10,** 785(2020), https://doi.org/10.3390/biom10050785
9. P. V. Kamat, R. Huehn, and R. Nicolaescu. *Journal of Physical Chemistry B,* **106,** 788(2002), https://doi.org/10.1021/jp013602t

10. Y. Bai, L. Zhou, K. Ma, H. Zhou, and Y. Xin. *Separation and Purification Technology,* **226,** 278(2019), https://doi.org/10.1016/j.seppur.2019.05.030
11. Y. Zhang, H. Liu, B. Guo, and J. Li. *Journal of Cleaner Production,* **420,** 140125(2025), https://doi.org/10.1016/j.jclepro.2025.140125
12. H. Najafian, F. Manteghi, F. Beshkar, and M. Salavati-Niasari. *Separation and Purification Technology,* **209,** 6(2019), https://doi.org/10.1016/j.seppur.2018.07.010
13. D. Yadesa, J. N. Guyasa, and T. T. Beyene. *Advances in Materials Science and Engineering,* **2024,** 4275035(2024), https://doi.org/10.1155/2024/4275035
14. I. Khan, K. Saeed, and I. Khan. *Arabian Journal of Chemistry,* **12,** 908(2019), https://doi.org/10.1016/j.arabjc.2017.05.011
15. E. S. Araújo, M. F. Pereira, G. M. da Silva, G. F. Tavares, C. Y. Oliveira, and P. M. Faia. *Toxics,* **11,** 658(2023), https://doi.org/10.3390/toxics11080658
16. B. Hameeda, A. Mushtaq, M. Saeed, A. Munir, U. Jabeen, and A. Waseem. *Toxin Reviews,* **40,** 1396(2021), https://doi.org/10.1080/15569543.2020.172557
17. B. K. Bellanthudawa, N. M. Nawalage, H. M. Handapangoda, S. Suvendran, K. A. Wijayasenarathne, M. L. Rathnasuriya, P. G. Wickramasinghe, A. A. Aberathna, A. Tennakoon, and I. Perera. *Nanotechnology for Environmental Engineering,* **8,** 975(2023), https://doi.org/10.1007/s41204-023-00291-2
18. S. S. Narender, V. V. Varma, C. S. Srikar, J. Ruchitha, P. A. Varma, and B. V. Praveen. *Chemical Engineering and Technology,* **45,** 397(2022), https://doi.org/10.1002/ceat.202100376
19. A. Saravanan, P. S. Kumar, S. Jeevanantham, S. Karishma, B. Tajsabreen, P. R. Yaashikaa, and B. Reshma. *Chemosphere, 280*, 130595(2021), https://doi.org/10.1016/j.chemosphere.2021.130595
20. S. A. Alsherari. *Journal of Materials Science: Materials in Electronics,* **35**, 983(2024), https://doi.org/10.1007/s10854-024-12718-x
21. C. H. Nguyen, M. L. Tran, T. T. V. Tran, and R.-S. Juang. *Separation and Purification Technology, 232*, 115962(2020), https://doi.org/10.1016/j.seppur.2019.115962
22. R. A. Senthil, M. Sun, J. Pan, S. Osman, A. Khan, and Y. Sun. *Optical Materials,* **92,** 284(2019), https://doi.org/10.1016/j.optmat.2019.04.003
23. M. Sudha, S. Surendhiran, V. Gowthambabu, A. Balamurugan, R. Anandarasu, Y. A. Syed Khadar, and D. Vasudevan. *Journal of Bio- and Tribo-Corrosion,* **7,** 60(2021), https://doi.org/10.1007/s40735-021-00492-w
24. Q. Yu, X. Ma, M. Wang, C. Yu, and T. Bai. *Applied Surface Science,* **254,** 5089(2008), https://doi.org/10.1016/j.apsusc.2008.02.065
25. O. M. Khubiev, A. R. Egorov, A. A. Kirichuk, V. N. Khrustalev, A. G. Tskhovrebov, and A. S. Kritchenkov. *International Journal of Molecular Sciences,* **24,** 10738(2023), https://doi.org/10.3390/ijms241310738
26. E. R. Beach, K. Shqau, S. E. Brown, S. J. Rozeveld, and P. A. Morris. *Materials Chemistry and Physics,* **115,** 371(2009), https://doi.org/10.1016/j.matchemphys.2008.11.016
27. J. Wang, W. D. Zhang, W. X. Ouyang, and Y. X. Yu. *Materials Letters,* **154**, 44(2015), https://doi.org/10.1016/j.matlet.2015.03.070
28. V. Biju and M. A. Khadar. *Spectrochimica Acta Part A,* **59,** 121(2003), https://doi.org/10.1016/S1386-1425(02)00291-4
29. M. Allali, M. A. Dahamni, M. Ghamnia, A. Boukhachem, D. Boukrédimi, D. Tonneau, and C. Fauquet. *Catalysts,* **12**, 931(2022), https://doi.org/10.3390/catal12090931
30. S. C. Chopade, I. G. Kore, S. P. Patil, N. D. Jadhav, C. Srinidhi, and P. A. Desai. *Ceramics International,* **44,** 5621(2018), https://doi.org/10.1016/j.ceramint.2017.12.177
31. A. Telfah, M. S. Mousa, M. J. Ahmad, C. J. Tavares, and R. Hergenröder. *Journal of Applied Polymer Science,* **139**, e52433(2022), https://doi.org/10.1002/app.52433

32. J. M. Musthafa and B. K. Mandal. *Photochemical and Photobiological Sciences,* **23,** 1(2024), https://doi.org/10.1007/s43630-024-00653-z
33. U. Punitha and A. M. Saral. *Results in Chemistry,* **7,** 101289(2024), https://doi.org/10.1016/j.rechem.2023.101289
34. P. S. Kumar, R. Sivakumar, S. Anandan, J. Madhavan, P. Maruthamuthu, and M. Ashokkumar. *Water Research,* **42,** 4878(2008), https://doi.org/10.1016/j.watres.2008.09.027
35. S. Anandan, P. S. Kumar, N. Pugazhenthiran, J. Madhavan, and P. Maruthamuthu. *Solar Energy Materials and Solar Cells,* **92**, 929(2008), https://doi.org/10.1016/j.solmat.2008.02.020

[RJC-9435/2025]